Observation of a core-excited $E4$ isomer in ^{98}Cd

A. Blazhev,[1,2] M. Górska,[1,3] H. Grawe,[1] J. Nyberg,[4] M. Palacz,[5] E. Caurier,[6] O. Dorvaux,[6] A. Gadea,[7] F. Nowacki,[6] C. Andreoiu,[8,*] G. de Angelis,[7] D. Balabanski,[2,†] Ch. Beck,[6] B. Cederwall,[9] D. Curien,[6] J. Döring,[1] J. Ekman,[8] C. Fahlander,[8] K. Lagergren,[9] J. Ljungvall,[4] M. Moszyński,[10] L.-O. Norlin,[9] C. Plettner,[1] D. Rudolph,[8] D. Sohler,[11] K. M. Spohr,[12] O. Thelen,[13] M. Weiszflog,[14] M. Wisell,[14] M. Wolińska,[5] and W. Wolski[10]

[1]*GSI, Planckstrasse 1, D-64291 Darmstadt, Germany*
[2]*University of Sofia, Sofia, Bulgaria*
[3]*Katholieke Universiteit Leuven, Leuven, Belgium*
[4]*Department of Radiation Sciences, Uppsala University, Uppsala, Sweden*
[5]*Heavy Ion Laboratory, Warsaw University, Warsaw, Poland*
[6]*IReS, Strasbourg, Cedex 2, France*
[7]*INFN Laboratori Nazionali di Legnaro, Legnaro, Italy*
[8]*Division of Cosmic and Subatomic Physics, Lund University, Sweden*
[9]*Department of Physics, Royal Institute of Technology, Stockholm, Sweden*
[10]*Soltan Institute for Nuclear Studies, Świerk, Poland*
[11]*Institute of Nuclear Research, Hungarian Academy of Science, Debrecen, Hungary*
[12]*University of Paisley, Paisley, Scotland*
[13]*IKP, Universität zu Köln, Köln, Germany*
[14]*Department of Neutron Research, Uppsala University, Uppsala, Sweden*

(Received 27 February 2004; published 3 June 2004)

A core-excited $I^{\pi}=(12^{+})$ spin-gap isomer was identified in ^{98}Cd in an experiment at EUROBALL IV. It was found to feed the known $I^{\pi}=(8^{+})$ seniority isomer by an $E4$ transition. Half-lives of $T_{1/2}=0.23\binom{+4}{-3}$ μs and $0.17\binom{+6}{-4}$ μs were measured for the two states at $E_x=6635$ keV and 2428 keV, respectively. From the excitation energy of the core-excited isomer a ^{100}Sn shell gap of 6.46(15) MeV is inferred. The measured $E4$ and $E2$ strengths, ^{100}Sn core excitations and the origin of empirical polarization charges are discussed in the framework of large-scale shell model calculations. An $E2$ polarization charge for protons of $\delta e_{\pi}<0.4\ e$ is found, which corresponds to the empirical value $\delta e_{\pi}=0.45\binom{+20}{-25}\ e$ in the pure proton hole valence space.

DOI: 10.1103/PhysRevC.69.064304 PACS number(s): 21.60.Cs, 23.20.Lv, 27.60.+j

I. INTRODUCTION

Doubly magic nuclei far off the stability line have been subject to many theoretical studies with respect to their shell structure and single particle energies [1], their susceptibility to core polarization and coupling to the continuum [2], and to realistic interactions derived from the free *NN* interaction by *G*-matrix-based many-body theory [3–5]. Therefore ^{100}Sn, the heaviest $N=Z$ doubly magic nucleus, and in addition to ^{48}Ni [6], the only doubly magic nucleus situated at the proton dripline provides an excellent study ground of these topics.

Since the first observation of excited states in ^{98}Cd via population of an $I^{\pi}=(8^{+})$ isomer [7] in a fusion-evaporation reaction, the extremely small proton polarization charge $\delta e_{\pi}<0.1\ e$ as derived, assuming a pure proton hole valence configuration, from the measured half-life was a puzzling fact. Moreover, a follow-up experiment employing fragmentation and in-flight separation [8] yielded a much shorter half-life and $\delta e_{\pi}=0.3\ e$. A solution to this puzzle was proposed by invoking the existence of a second, core-excited $I^{\pi}=12^{+}$ isomer, which in fusion-evaporation reactions is populated with much larger cross section (isomeric ratio) than in fragmentation [9]. Recently below $Z=N=50$ a number of spin-gap isomers were identified [10–12], which cannot be explained in the minimum valence space $\pi\nu(p_{1/2},g_{9/2})$ but require excitations of the ^{100}Sn core [13]. The identification of core-excited states in ^{98}Cd combined with a shell-model estimate of residual interactions provides a very direct measure of the ^{100}Sn shell gap [9]. Estimates for this value have been obtained so far by a shell-model based extrapolation from ^{90}Zr [14] and a shell-model analysis of core-excited states in ^{99}Cd and ^{101}In [15].

In the present paper the identification of a core-excited isomer in ^{98}Cd, its interpretation in large-scale shell model calculations and an inferred measure for the ^{100}Sn shell gap are described. Implications for the susceptibility of the ^{100}Sn core to $E2$ polarization and the existence of long-lived core-excited isomers in and around ^{100}Sn are discussed. The search for prompt-delayed coincident new γ-ray transitions will be described in a forthcoming paper.

II. EXPERIMENT AND ANALYSIS

A fusion-evaporation reaction is the most effective way to study in-beam the structure of nuclei in the ^{100}Sn region. A

*Present address: Department of Physics, University of Guelph, Guelph, Ontario, Canada NIG 2W1.

†Present address: Dipartimento di Fisica, Università degli Studi de Camerino, Camerino, Italy.

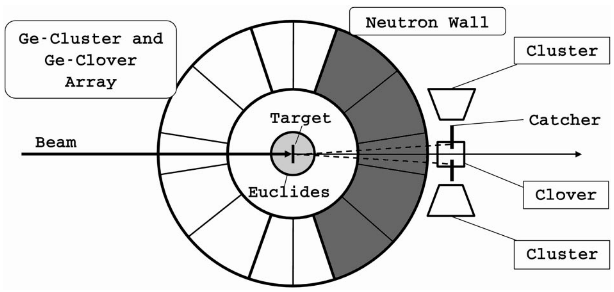

FIG. 1. Schematic sketch of the experimental setup.

pulsed beam of ^{58}Ni served as projectile and as a time reference for the ^{46}Ti(^{58}Ni,$\alpha 2n$)^{98}Cd reaction. The pulse repetition time was $\Delta t = 330$ ns. The ^{46}Ti target of 1 mg/cm^2 thickness was made of a material enriched to 86%. The EUROBALL [16] spectrometer consisting of 26 Clover [17] and 15 Cluster detectors [18] was used in combination with the EUCLIDES [19] Si ball and the neutron wall [20]. In this way the identification of the reaction channel was assured and prompt γ rays emitted directly from the target were measured. Downstream from the thin target, at a distance of 1.19 m, a catcher foil was mounted where the recoiling nuclei were stopped after a flight time of about 100 ns. The experimental setup is schematically shown in Fig. 1.

The foil had an inner hole to let the noninteracting beam particles pass through. Around the catcher an array of two cluster and one clover detectors was placed in a close geometry to assure high efficiency for gamma rays from decaying isomeric states which lived long enough to survive the flight time between the target and the stopper. An event from data acquisition was accepted whenever at least one gamma ray (prompt or delayed within 1500 ns) was registered together with at least one prompt neutron prediscriminated from γ rays detected in the neutron wall by hardware pulse shape analysis. The whole data set was scanned for possible gain and time shifts and matched with the help of the program ALIGN [21]. The efficiency of the γ-ray spectrometer around the target was 6.6% in this configuration and 2.8% for the downstream array at 1.3 MeV γ-ray energy after applying add back. The energy and efficiency calibrations were performed using standard sources (i.e., ^{56}Co, ^{152}Eu, and ^{133}Ba). The energy calibration of the downstream array above 3.5 MeV was analyzed via comparison of extrapolations of first and second order polynomial fits and accounting for the energies of the single escape peaks. The absolute efficiency of the downstream array was estimated relative to the target array (clusters and clovers). The catching efficiency amounted to about 40% for the case of ^{98}Cd. This was estimated from the simulation code PACE [22], which includes reaction kinematics, slowing down, and multiple scattering processes in the target. The neutron efficiency of the neutron wall was 25%. The charged particle efficiencies of the EUCLIDES array were different in coincidence with γ rays from the target and those measured around the catcher foil. This is a result of the correlated detection efficiency for evaporated charged particles in coincidence with residues hitting the catcher, due to reaction kinematics. The catcher covers the most forward part of the recoil cone corresponding to preferential forward and backward particle emission, where their detection efficiency is reduced due to the holes in the EUCLIDES array for the beam entrance and exit, and due to the absorption in detector absorber at low energy of the evaporated particle. Therefore the effect is the highest when the recoiling nucleus was created after an α-particle evaporation. The efficiencies of the EUCLIDES array based on γ rays emitted at the target (catcher) position were 60% (55%) for protons and 40% (15%) for α particles.

The experimental setup and the structure of the data allowed to collect coincidence spectra between prompt and delayed, prompt-prompt, and delayed-delayed γ rays gated with different particle conditions. The time window for the delayed γ rays was optimized between 90 and 1240 ns after arrival of the beam pulse on target, which accounts for the target-catcher flight time of recoils and γ's. The single γ-ray spectra with various combinations of coincident particles were used for the identification of the reaction exit channel. In the analysis the software packages RADWARE [23] and ROOT [24] were used.

III. RESULTS

A. $\gamma\gamma$ and particle-γ coincidences

The four known γ-ray transitions [7] were observed in the delayed spectra and their origin from ^{98}Cd was again confirmed. However, in the higher energy part of the particle gated spectra a new line at 4207 keV was observed. This part of the γ-ray spectra created with different particle conditions is shown in Fig. 2.

From the appearance of this line in the $0\alpha 0p1n$ [Fig. 2(a)], $1\alpha 0p1n$ [Fig. 2(c)], $0\alpha 0p2n$ [Fig. 2(d)], and $1\alpha 0p2n$ [Fig. 2(e)] gated spectra, and its absence in the $0\alpha 1p1n$ [Fig. 2(b)] gated spectrum it was deduced that the transition occurs in a nucleus produced in an $\alpha 2n$ exit channel. The line was not visible in the 2α-gated spectra, but due to the very low efficiency for the α particles in coincidence with γ rays emitted at the catcher position (see above) it was very difficult to make a firm conclusion. Inspection of the coincidence matrices proves that this high-energy line is in delayed coincidence with the other four transitions belonging to ^{98}Cd, as demonstrated in Fig. 3.

To exploit the full statistics all possible particle conditions were used for the summed energy and time spectra, namely, $0\alpha 0p1n$, $0\alpha 0p2n$, $0\alpha 0p3n$, $1\alpha 0p0n$, $1\alpha 0p1n$, $1\alpha 0p2n$, and $1\alpha 0p3n$. Since discrimination of the scattered neutrons was not applied, the $3n$ condition also provides γ rays correlated with the $(1\alpha 2n)$ exit channel.

B. Time spectra and half-life analysis

Three different methods have been employed to determine half-life values and limits for the isomers at 6635, 2428, and 2281 keV excitation energy (Table I). The background subtraction and the fitting procedure were optimized analyzing the decay of the $I^{\pi}=8^{+}$ isomer in ^{100}Cd, which yielded a half-life value of $T_{1/2}=61(1)$ ns in good agreement with Ref. [25].

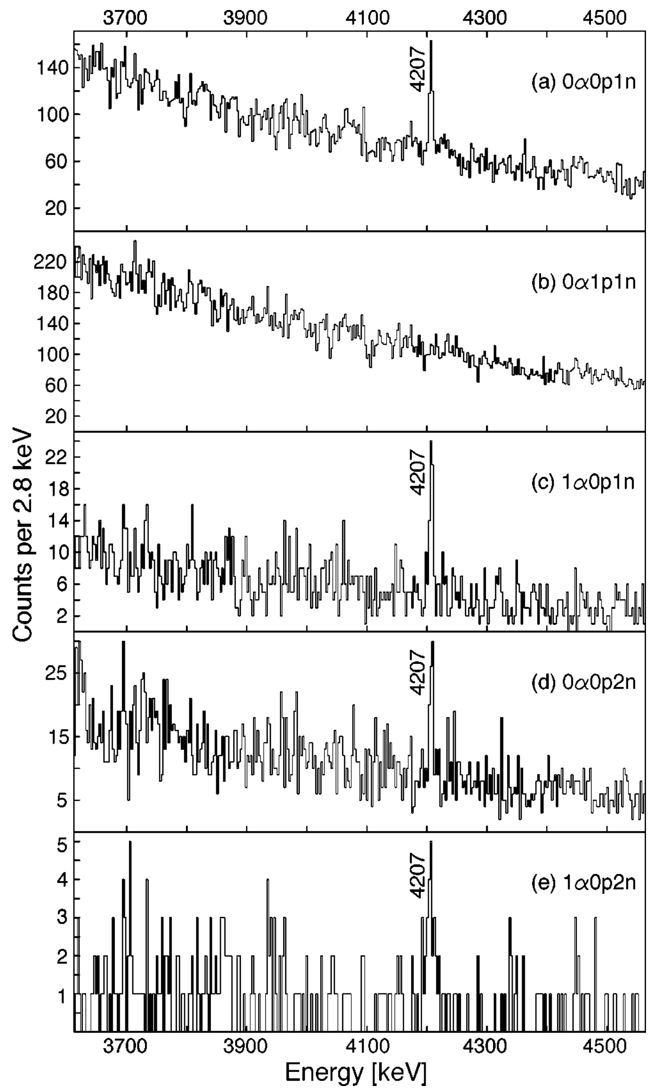

FIG. 2. High-energy portion of the γ-ray spectrum gated by various conditions on evaporated particles as follows: (a) $0\alpha0p1n$, (b) $0\alpha1p1n$, (c) $1\alpha0p1n$, (d) $0\alpha0p2n$, (e) $1\alpha0p2n$.

Figure 4 shows the background subtracted time-delay spectrum with reference to the beam pulse on target for the new 4207 keV γ ray, which precedes the known $I^{\pi}=(8^{+})$ isomer. The half-life resulting from a single exponential fit is $T_{1/2}=230\binom{+40}{-30}$ ns. This value along with the strong feeding intensity (Table I) explains the long apparent half life inferred previously in a similar experiment for the $I^{\pi}=(8^{+})$ state [7].

In view of this fact, the similarity of the lifetimes involved and the experimental uncertainties it is not promising to apply the same method to the time distribution of the 1395 keV γ ray to infer the $I^{\pi}=(8^{+})$ half-life from a two exponential component fit. Therefore this lifetime was determined from a $\gamma\gamma(t)$ time distribution with start on the feeding 4207 keV line and stop by the 688 keV and/or 1395 keV γ rays below the $I^{\pi}=(8^{+})$ isomer. The time spectrum shown in Fig. 5 is virtually background free, and from a single exponential fit a half-life $T_{1/2}=170\binom{+60}{-40}$ ns was determined. The additional delay in the $I^{\pi}=(6^{+})$ state (see below) will enlarge the error bars given above only marginally. Within these error bars the value agrees well with the result from a previous fragmentation experiment [8].

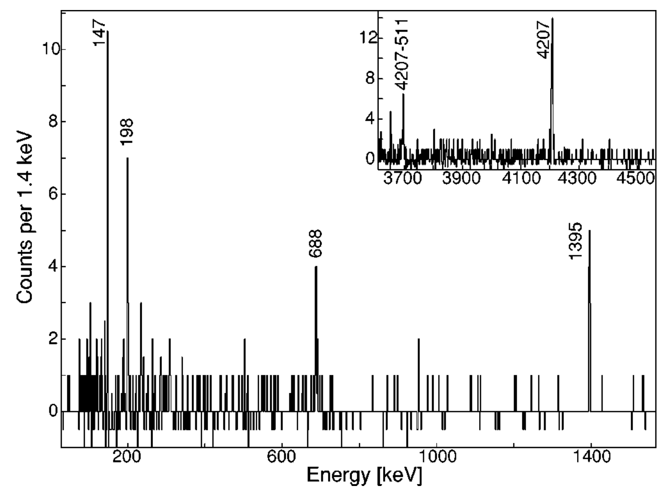

FIG. 3. Spectrum gated on the 4207 keV line. The inset shows the high-energy part of the cross coincidence spectrum created by the sum of gates on the 147, 198, 688, and 1395 keV lines with particle condition $0\alpha0p1n$, $0\alpha0p2n$, $0\alpha0p3n$, $1\alpha0p0n$, $1\alpha0p1n$, $1\alpha0p2n$, and $1\alpha0p3n$ and with unresticted coincidence time window.

It has been stated before that from nuclear structure arguments a half-life for the $I^{\pi}=(6^{+})$ state in the 10–20 ns range is expected [7]. This is too short for a $\gamma\gamma(t)$ delay curve analysis, since low-energy γ rays, which are subject to large time walk, are involved. Therefore the centroid shift method [26] was applied in this case. In Fig. 6 the centroids of the low-energy 147 and 198 keV γ-ray time distributions gated by coincidence with the 1395 keV γ ray are shown. The time-zero line is determined from the time distribution of the Compton background, which is known to provide a good reference [26]. As expected from the decay scheme (Fig. 7) the 198 keV line is prompt, while the 147 keV centroid is clearly shifted. A limit on the half-life, $T_{1/2}<20$ ns, is deduced from this shift at a 2σ confidence level.

C. Level scheme and spin-parity assignments

Based on the coincidence relations, the γ-ray intensities and the half-lives (Table I), the decay scheme shown in Fig. 7 is proposed. This implies that the high-energy γ ray is the

TABLE I. Level energies, spin-parity assignments, half-lives, γ-ray energies, and intensities.

E_x [keV]	I_i^{π}	$T_{1/2}$ [ns]	E_{γ} [keV]	I_{γ} [%]	I_f^{π}
1395	(2^{+})		1394.9(2)	100(15)	0^{+}
2083	(4^{+})		687.8(3)	105(15)	(2^{+})
2281	(6^{+})	<20	198.2(2)	80(15)	(4^{+})
2428	(8^{+})	$170\binom{+60}{-40}$	147.1(2)	70(15)	(6^{+})
6635	(12^{+})	$230\binom{+40}{-30}$	4207(2)	50(35)	(8^{+})

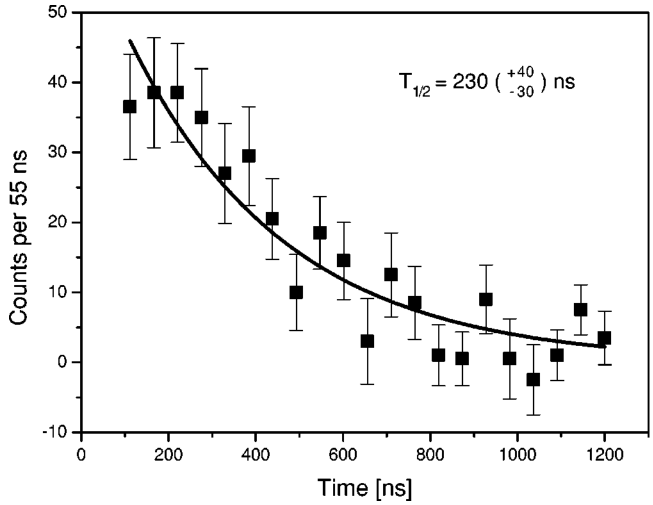

FIG. 4. Background subtracted time spectrum of the 4207 keV line with particle gates on $0\alpha0p1n$, $0\alpha0p2n$, $0\alpha0p3n$, $1\alpha0p0n$, $1\alpha0p1n$, $1\alpha0p2n$, and $1\alpha0p3n$. The fit region is 105–1240 ns with reference to the beam pulse on target.

primary $E4$ isomeric transition. An odd-parity assignment is discarded on the following grounds: (i) Excitations to the $h_{11/2}$ orbit are expected to be at least 2.5 MeV above those to the $d_{5/2}$ and $g_{7/2}$ orbitals [27] and (ii) the coupling of a possible low-lying $I^{\pi}=3^-$ state in ^{100}Sn [28] to the 8^+ isomer would decay back by a nonisomeric high-energy $E3$ transition. On the other hand, the $E1$ transition of a 12^+ state to such an 11^- state would be highly configuration hindered due to particle and l forbiddance. Alternatives for the spin-parity assignment to the new isomer and its γ decay require the existence of a nonobserved highly converted primary $E2$ transition. The close structural analogy between ^{100}Sn and ^{56}Ni [9,29] would suggest a $12^+\rightarrow10^+\rightarrow8^+$ sequence as inferred from the analogous $10^+\rightarrow8^+\rightarrow6^+$ cascade in ^{54}Fe with an $E2/E4$ branching ratio of 54:1 [30,31]. From the present spectra (Figs. 2 and 3) the branching of a second

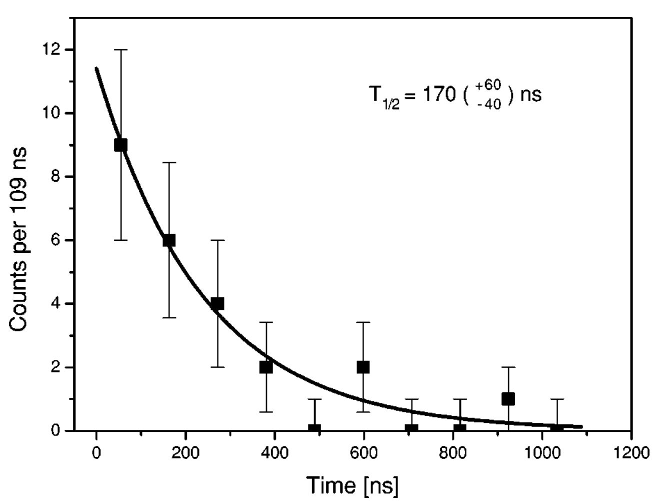

FIG. 5. Time delay spectrum $\gamma\gamma(t)$ with start on 4207 keV γ ray and stop on OR of 688 and 1395 keV γ rays. (Particle gate on $0\alpha0p1n$, $0\alpha0p2n$, $0\alpha0p3n$, $1\alpha0p0n$, $1\alpha0p1n$, $1\alpha0p2n$, and $1\alpha0p3n$.)

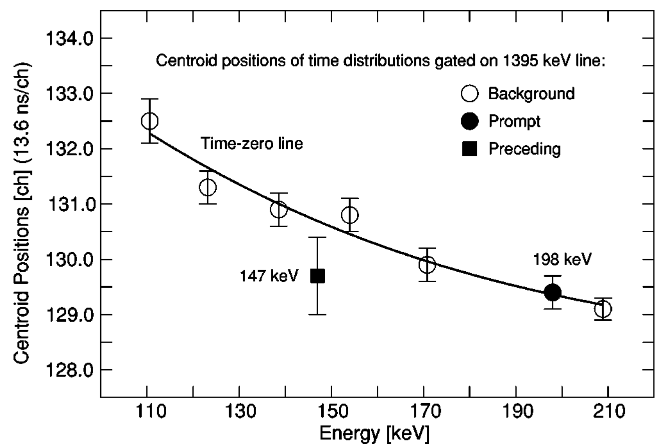

FIG. 6. Time-zero line of γ's in coincidence with the 1395 keV line. The reference line is a fit to the centroids of the time distributions for prompt coincidence. The energy dependence reflects the time walk. The centroid shift of the 147 keV line compared to the time-zero line (time of 198 and 1395 keV lines) is a direct measure of the 6^+ state lifetime. (Particle gate on $0\alpha0p1n$, $0\alpha0p2n$, $0\alpha0p3n$, $1\alpha0p0n$, $1\alpha0p1n$, $1\alpha0p2n$, and $1\alpha0p3n$.)

high-energy γ-ray within ±100 keV of the 4207 keV transition can be restricted to be <10%. The dominance of the $E2$ branch in ^{54}Fe after proper scaling with mass A (radius dependence of EL operator), transition energies (E_{γ}^{2L+1}) and internal conversion reduces to less than 1:1 in ^{98}Cd assuming an 80 keV lower observational limit for the $E2$ transition. Based on the assumption of an unchanged relative reduced $E4$ and $E2$ strength between ^{56}Ni and ^{100}Sn, this is at variance with the experimental observation of one dominating transition. Therefore the hypothetical 10^+ would lie either less than 80 keV below the 12^+ state, or above, leaving an $E4$ assignment for the observed 4207 keV transition. A second alternative consistent with the observed γ decay, a $14^+\rightarrow12^+\rightarrow8^+$ sequence, is unique for ^{100}Sn and has no counterpart in ^{54}Fe. Due to the near degeneracy of the $d_{5/2}$ and $g_{7/2}$ neutron orbits [27] the $I^{\pi}=14^+$ state of configuration $\pi(g_{9/2})_{8^+}\nu g_{9/2}^{-1}g_{7/2}$ can come very close to the $I^{\pi}=12^+$ state involving the $d_{5/2}$ orbital. The corresponding 12^+ state in ^{54}Fe cannot be isomeric as the $\nu p_{3/2}-f_{5/2}$ splitting is 1.03 MeV in ^{56}Ni [27]. In conclusion $E4$ character was inferred for the 4207 keV primary γ ray originating from an $I^{\pi}=(12^+)$ state. From the present data, however, the existence of a 10^+ and/or 14^+ state close below and/or above the $I^{\pi}=(12^+)$ isomer cannot be excluded. For further discussion see Sec. IV B.

IV. DISCUSSION

A. Shell model calculation

To address the issues outlined in the Introduction (Sec. I) shell-model calculations were performed in two different approaches that will be described below. The nucleus ^{100}Sn has been used as an inert core in numerous shell-model calculations (see Ref. [27] for a recent review) and derivations of realistic interactions [3–5]. From the striking similarity of its

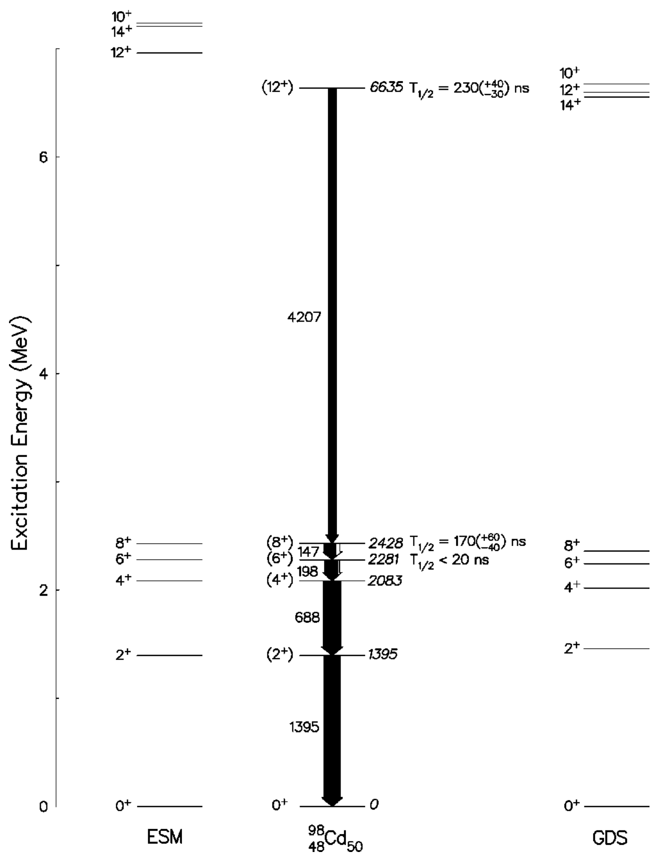

FIG. 7. Experimental level scheme of ^{98}Cd in comparison to empirical shell model results in the pure configuration $\pi g_{9/2}^{-2} \nu g_{9/2}^{-1} d_{5/2}$ (ESM) and in the full $\pi\nu(gds)$ model space at truncation level $t=4$ (GDS).

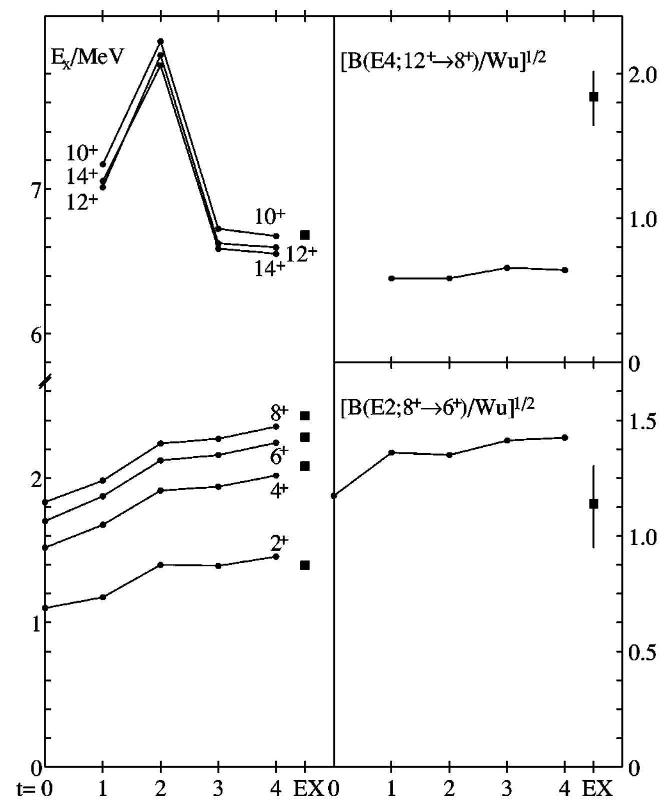

FIG. 8. Convergence of selected observables with truncation level t in the GDS calculation. Note the broken energy scale between 2 and 6 MeV.

single-particle structure to ^{56}Ni [27], one major shell below, it can be inferred, however, that its ground state contains a similar percentage of multiple particle-hole (ph) excitations as ^{56}Ni [32,33]. On the other hand, particle-hole shell-model calculations in minimum model spaces using empirical interactions were performed for $N \leqslant 50$ nuclei to account for core-excited states [34] and Gamow-Teller β decay [35,36]. In the present paper we employ these two extreme approaches to enlighten the experimental data on core-excited states and electromagnetic transition rates.

1. Large-scale shell model (LSSM)

With the availability of large-scale shell model codes such as ANTOINE [37,38] and NATHAN [38–40] it has become possible to perform untruncated calculations with monopole corrected interactions in the (p,f) shell up to ^{60}Zn [41], which makes an extension to ^{100}Sn including *np-nh* excitations a new challenge. We have chosen the (gds) model space comprising the $0g$, $1d$, and $2s$ orbitals above a hypothetical ^{80}Zr core using a realistic G-matrix based interaction as described in Ref. [3]. As ^{80}Zr in its ground state is not spherical, single-particle energies were estimated from the global predictions of Ref. [42]. Monopole corrections were applied to reproduce the extrapolated single-particle/hole energies of ^{100}Sn [27] including a shell gap of 6.50 MeV. The higher multipoles were scaled by a factor of 1.15 yielding a consistent description of the core-excited isomers in the region [12]. Effective $E2$ and $E4$ polarization charges of 0.5 e were used to calculate transition rates. In Fig. 8 the convergence of the shell model with the number of ph excitations t included in the calculations is shown (t is referred to as the truncation level). Clearly at $t=4$ near convergence has been reached for all observables. Therefore time consuming calculations with $t>4$ were not performed. The final results, further on referred to as GDS, are shown in Fig 7 and discussed in Sec. IV B.

2. Empirical shell model (ESM)

In an alternative empirical approach the pure configurations $\pi g_{9/2}^{-2}$ and $\pi g_{9/2}^{-2} \nu g_{9/2}^{-1} d_{5/2}$ were assumed for the proton valence space and the core-excited states, respectively. The $\pi g_{9/2}^{-2}$ TBME were taken from the experimental ^{98}Cd spectrum and the $\pi g_{9/2}^{-1} \nu g_{9/2}^{-1}$, $\pi g_{9/2}^{-1} \nu d_{5/2}$, and $\nu g_{9/2}^{-1} d_{5/2}$ interaction energies from ^{90,92}Nb and ^{90}Zr [30] using the Pandya transformation to convert pp into ph TBME. The shell gap was taken as 6.78 MeV [27] and configuration mixing was neglected.

B. Comparison to experiment

1. Level energies and ^{100}Sn shell gap

In Fig. 7 the experimental decay scheme of the $I^{\pi}=(12^+)$ and (8^+) isomers is compared to the results of the

LSSM calculation at $t=4$ (GDS) and the empirical ESM approach. The two-proton hole valence levels of predominant (68%) $\pi g_{9/2}^{-2}$, $I^{\pi}=0^{+}-8^{+}$, which serve in the ESM approach as input, are excellently accounted for by the GDS calculation.

The excitation energy of the core excited $I^{\pi}=12^{+}$ isomer is determined by the ^{100}Sn neutron shell gap, which in the GDS calculation is adopted to be identical to the proton gap as can be inferred from a comparison to ^{56}Ni [9], and by the interaction energy in the leading configurations $\pi g_{9/2}^{-2}\nu g_{9/2}^{-1}(d_{5/2},g_{7/2})$. The latter is dominated by the strongly binding $\pi g_{9/2}^{-2}\nu g_{9/2}^{-1}$ interaction energy, which is approximately equal to the $\pi g_{9/2}^{-2}$ pairing energy (see, e.g., Ref. [29]). Therefore the excitation energy of the isomer is a direct measure of the ^{100}Sn shell gap. This is corroborated by the analogous situation in ^{56}Ni, namely, the $I^{\pi}=10^{+}$ isomer in ^{54}Fe at $E_x=6527$ keV [31] as compared to an average 6.410 MeV shell gap for protons and neutrons [29]. In the present shell-model approaches shell gaps of 6.50 MeV (GDS) and 6.78 MeV (ESM) were adopted. From a comparison to the experimental core-excitation energy as documented in the $12^{+}\rightarrow 8^{+}$ transition energy values of 6.47 MeV (GDS) and 6.46 MeV (ESM) are inferred to match theory and experiment. Therefore an average value of 6.46(15) MeV is adopted for the shell gap with the error stemming from systematic model and interaction dependent uncertainties including a contribution by an unobserved low-energy γ-ray transition (see Secs. III and IV B 2). The value is in good agreement with previously quoted values and uncertainties [14,15] but much less affected by systematic ambiguities.

The level sequence in the GDS calculation suggests the existence of an $I^{\pi}=14^{+}$ $E6$ yrast trap, which is stable in its position for $t>1$ (Fig. 8). Inspection of the wave functions reveal a leading configuration $\pi g_{9/2}^{-2}\nu g_{9/2}^{-1}g_{7/2}$ for this state in contrast to the $\pi g_{9/2}^{-2}\nu g_{9/2}^{-1}d_{5/2}$ configuration for the $I^{\pi}=12^{+}$ state. This explains the deviating sequence in the ESM estimate, which excludes the $\nu g_{7/2}$ orbit. On the other hand the results for ^{101}Sn for all levels of truncation reproduce the extrapolated $\nu d_{5/2}$-$g_{7/2}$ splitting, which is inferred from the experimental ^{103}Sn single-particle states [43,44]. The existence of an $I^{\pi}=14^{+}$ yrast trap cannot be excluded by the evidence from the present experiment. An $E6$ γ-ray branch would not compete with β decay and, moreover, due to the long half-life (0.1–1 s) would exceed the maximum observational time range limit of 1.2 μs covered in the present experiment. A possible $12^{+}\rightarrow 14^{+}$ branch would escape observation due to high internal conversion and the weak $E2$ transition strength (see Sec. IV B 2).

2. Electromagnetic transitions and *E*2 polarization charges

In Table II $E2$ and $E4$ transition strengths as calculated in the GDS approach at $t=4$ are listed and compared to experiment. For the high-spin isomer, in addition to the most likely 12^{+} assignment and $E4$ isomerism, the options of highly converted $E2$ transitions $12^{+}\rightarrow 10^{+}$ and $14^{+}\rightarrow 12^{+}$ are listed with lower limits based on the observational limit of $E_{\gamma}>80$ keV. In spite of the large experimental uncertainties in the present work it seems that the GDS calculation with standard polarization charges 0.5 e overestimates the $8^{+}\rightarrow 6^{+}$ $E2$ strength.

TABLE II. Experimental and shell model $E2$ and $E4$ strengths in Weisskopf units (for $E2$: 1 W.u.$=26.84e^2$ fm^4 and for $E4$: 1 W.u.$=12830e^2$ fm^8). Polarization charges of 0.5e were used for the $E2$ and $E4$ operator, respectively.

$I_i^{\pi}\rightarrow I_f^{\pi}$	E_{γ} [keV]	σL	GDS [W.u.]	EXP [W.u.]
$6^{+}\rightarrow 4^{+}$	198	$E2$	5.14	>3
$8^{+}\rightarrow 6^{+}$	147	$E2$	2.03	1.3(4)
				1.1(2)[a]
$12^{+}\rightarrow 8^{+}$	4207	$E4$	0.41	3.4(7)
$14^{+}\rightarrow 12^{+}$	<80	$E2$	0.20	>4.9[b]
$12^{+}\rightarrow 10^{+}$	<80	$E2$	0.69	>4.9[c]
$10^{+}\rightarrow 8^{+}$		$E2$	0.013	

[a]Reference [8].
[b]Alternative decay sequence $14^{+}\rightarrow 12^{+}\rightarrow 8^{+}$.
[c]Alternative decay sequence $12^{+}\rightarrow 10^{+}\rightarrow 8^{+}$.

This is even more apparent in comparison to a previous measurement of much higher statistical precision [8], which in view of the present work may, however, be subject to systematic errors due to the unknown feeding by the core-excited isomer. Therefore we infer from the present work an upper limit $\delta e_{\pi}<0.4\ e$ for the proton polarization charge. The $B(E2)$ value quoted in Ref. [8] would correspond to the more stringent limit of $\delta e_{\pi}<0.2\ e$. The neutron contributions were corrected for by assuming the LSSM values with $e_{\nu}=0.5\ e$. This has to be compared to the two-neutron nucleus ^{102}Sn. An $E2$ transition strength has been measured to be $B(E2;6^{+}\rightarrow 4^{+})=116^{+70}_{-30}\ e^2$fm^4 [45], from which with the GDS value 85 e^2 fm^4 at truncation level $t=4$ a neutron polarization charge $\delta e_{\nu}=0.6(1)\ e$ is deduced. This supersedes the value of Ref. [9] (SDG) which was obtained at $t=3$. These effective charges are in remarkable agreement with core polarization calculations, that predict a large isovector effect [46,47]. On the other hand, the simple formula quoted in Ref. [48] with reduced isovector strength, yielding $\delta e_{\pi}=0.33\ e$ and $\delta e_{\nu}=0.65\ e$, accounts for the experimental values. The $E2$ core polarization is made up from two contributions, a high-energy part due to $\Delta N=2$ *ph* excitations to the next harmonic oscillator (HO) shell with the same parity, i.e., the giant quadrupole resonance (GQR), and a soft part due to *ph* excitations within the valence HO shell, which can be calculated in the LSSM approach. Therefore, assuming convergence of the LSSM calculations, the extracted experimental limits and values reflect the GQR tail contribution to the effective charge and can be directly compared to the quoted theoretical predictions [46–48].

Very often effective charges are routinely extracted by assuming minimum model space valence configurations. These normally much larger empirical polarization charges contain the soft *ph* excitations and are very much dependent on the purity of the assumed valence configuration. On the theory side these values should be compared to RPA results based on Skyrme Hartree-Fock calculations [2]. The LSSM results on $E2$ strengths open an interesting insight into the microscopic nature of *ph* excitations and empirical effective charges. In a single-j shell ESM approach all $E2$ matrix elements are proportional to each other. For the $\pi g_{9/2}^{-2}$ configuration in ^{98}Cd this results, e.g., in the relation $B(E2;8\rightarrow 6):B(E2;6\rightarrow 4):Q^2(8)=1:2.50:38.3$, where Q is the spectroscopic quadrupole moment. The LSSM results preserve these ratios at all levels of truncation within $\sim$1%. This supports the idea of valence nucleons "dressed" by *ph* excitations and the concept of an effective charge. Another interesting result can be inferred from the comparison of the $t=0$ and $t=4$ $B(E2;I_{\rm max}\rightarrow I_{\rm max}-2)$ values for the proton and neutron valence nuclei ^{98}Cd ($I_{\rm max}=8$) and ^{102}Sn ($I_{\rm max}=6$), commonly believed to have rather pure configurations outside the ^{100}Sn closed shells [7,45], which in the LSSM calculations are well converged at $t=4$. The apparent empirical polarization charges as extracted from the theoretical $B(E2)$ values are $\delta e_\pi=0.86\,e$ and $\delta e_\nu=1.70\,e$. The large isovector effect is due to the empirical fact that valence protons (neutrons) are mainly polarised by neutron (proton) core excitation as can be inferred from inspection of the corresponding wave functions. The experimental values for the empirical effective polarization charge as deduced from the present work and Ref. [45], assuming pure proton hole and neutron particle valence configurations, are $\delta e_\pi=0.45\binom{+20}{-25}e$ and $\delta e_\nu=2.0\binom{+5}{-3}e$, respectively.

Shell-model predictions of $E4$ transition rates are hampered by the fact that little is known about the effective operator, i.e., the polarization charges. The GDS calculation underestimates the enhanced experimental value at least by a factor 6, if $E2$ charges are used (Table II). Though full convergence may not have been reached at $t=4$ in this case (Fig. 8), one can hardly expect more than a factor of 2 increase. Increase of the polarization charges within reasonable limits may account for another factor of 2, which is still a factor of 1.5–2.0 smaller than the experimental value. The aforementioned analogous $E4$ strength in ^{54}Fe $B(E4;10^+\rightarrow 6^+)=0.79(8)$ W.u. [30] is calculated to be 0.83 W.u. using the KB3 interaction [49] and 1.81Wu with FPD6 [50]. Both values are found to be converged at $t=6$. It is well known though that in the (p,f) shell $E4$ strengths are strongly interaction dependent [38], and thus provide a sensitive test ground.

The alternative $E2$ scenarios for the core-excited isomerism as discussed and discarded in Sec. III C are clearly at variance with the shell model results as they underestimate the lower experimental limits by a great margin (Table II) against the trend observed for the $8^+\rightarrow 6^+$ transition.

V. SUMMARY AND CONCLUSIONS

A core-excited spin-gap isomer was identified in ^{98}Cd and tentatively assigned as an $I^\pi=(12^+)$ state. Half-lives were determined for the $I^\pi=(12^+)$, (8^+), and (6^+) levels and discussed within the framework of empirical and large-scale shell model calculations. The ^{100}Sn shell gap was inferred from a comparison of the experimental and shell model excitation energy of the $I^\pi=(12^+)$ isomer. The LSSM including up to $4p4h$ excitations of the ^{100}Sn core is found to excellently account for the experimental observations. It is a challenge for future experiments to verify the predicted $I^\pi=14^+$ $E6$ isomer in ^{98}Cd and a possible $I^\pi=6^+$ $E2$ isomer in ^{100}Sn.

ACKNOWLEDGMENTS

The authors gratefully acknowledge the comments by J. Blomqvist to the nature of core-excited isomers near ^{56}Ni and ^{100}Sn. The authors appreciate the extraordinary technical assistance and support by the EUROBALL collaboration and the IReS staff. The Swedish coauthors acknowledge the help of the Swedish Research Council and the AIM Graduate Education Programme at Uppsala University. The work was partly supported by the EU under Contract No. HPRI-CT-1999-00078 and partly by the Polish Committee of Scientific Research (Grants No. 5P03B 046 20 and 1P03B 031 26).

[1] K. Rutz *et al.*, Nucl. Phys. **A634**, 67 (1998).
[2] I. Hamamoto and H. Sagawa, Phys. Lett. B **394**, 1 (1997).
[3] M. Hjorth-Jensen *et al.*, Phys. Rep. **261**, 125 (1995).
[4] F. Andreozzi *et al.*, Phys. Rev. C **54**, 1636 (1996).
[5] J. Sinatkas *et al.*, J. Phys. G **18**, 1377 (1992); **18**, 1401 (1992).
[6] B. Blank *et al.*, Phys. Rev. Lett. **84**, 1116 (2000).
[7] M. Górska *et al.*, Phys. Rev. Lett. **79**, 2415 (1997).
[8] R. Grzywacz, in *ENAM98: Exotic Nuclei and Atomic Masses*, edited by Bradley M. Sherill *et al.*, AIP Conf. Proc. No. 455 (AIP, Melville, 1998), p. 257.
[9] H. Grawe *et al.*, Nucl. Phys. **A704**, 211c (2002).
[10] M. La Commara *et al.*, Nucl. Phys. **A708**, 167 (2002).
[11] J. Döring *et al.*, Phys. Rev. C **68**, 034306 (2003).
[12] C. Plettner *et al.*, Nucl. Phys. **A733**, 20 (2004).
[13] H. Grawe, in *Proceedings of the International Workshop XXXI Gross Properties of Nuclei and Nuclear Excitations*, Hirschegg, Austria 2003, edited by H. Feldmeier, J. Knoll, W. Nörenberg, and J. Wambach (GSI, Darmstadt, 2003), p. 94.
[14] H. Grawe *et al.*, Phys. Scr. **T56**, 71 (1995).
[15] M. Lipoglavšek *et al.*, Phys. Rev. C **66**, 011302(R) (2002).
[16] J. Simpson, Z. Phys. A **358**, 139 (1997).
[17] G. Duchêne *et al.*, Nucl. Instrum. Methods Phys. Res. A **432**, 90 (1999).
[18] J. Eberth *et al.*, Nucl. Instrum. Methods Phys. Res. A **369**, 135 (1996).
[19] E. Farnea *et al.*, Nucl. Instrum. Methods Phys. Res. A **400**, 87 (1997).
[20] O. Skeppstedt *et al.*, Nucl. Instrum. Methods Phys. Res. A **421**, 531 (1999).
[21] M. Palacz *et al.*, Nucl. Instrum. Methods Phys. Res. A **383**, 473 (1996).
[22] K. M. Spohr *et al.* (unpublished).
[23] D. C. Radford, Nucl. Instrum. Methods Phys. Res. A **361**, 297 (1995); see also http://radware.phy.ornl.gov/
[24] R. Brun and F. Rademakers, Nucl. Instrum. Methods Phys. Res. A **389**, 81 (1997); see also http://root.cern.ch/

[25] M. Górska *et al.*, Z. Phys. A **350**, 181 (1994).
[26] W. Andrejtscheff *et al.*, Nucl. Instrum. Methods Phys. Res. **204**, 123 (1982).
[27] H. Grawe and M. Lewitowicz, Nucl. Phys. **A693**, 116 (2001).
[28] M. Górska *et al.*, Phys. Rev. C **58**, 108 (1998).
[29] H. Grawe *et al.*, in *Nuclear Structure 98*, edited by Cyrus Baktash, AIP Conf. Proc. No. 481 (AIP, Melville, 1999), p. 177.
[30] Evaluated Nuclear Data Structure File, http://www.nndc.bnl.gov/nndc/ensdf/
[31] M. H. Rafailovich *et al.*, Phys. Rev. C **27**, 602 (1983).
[32] T. Otsuka *et al.*, Phys. Rev. Lett. **81**, 1588 (1998).
[33] F. Nowacki, Nucl. Phys. **A704**, 223c (2002).
[34] K. Muto *et al.*, Phys. Lett. **135B**, 349 (1984).
[35] I. P. Johnston and L. D. Skouras, Eur. Phys. J. A **11**, 125 (2001).
[36] L. Batist *et al.*, Nucl. Phys. **A720**, 222 (2003).
[37] E. Caurier, code ANTOINE, Strasbourg, 1989.
[38] E. Caurier and G. Martínez-Pinedo, Nucl. Phys. **A704**, 60c (2002).
[39] E. Caurier and F. Nowacki, code NATHAN, Strasbourg, 1997.
[40] E. Caurier *et al.*, Phys. Rev. C **59**, 2033 (1999).
[41] C. Mazzocchi *et al.*, Eur. Phys. J. A **12**, 269 (2001); E. Caurier (private communication).
[42] J. Duflo and A. P. Zuker, Phys. Rev. C **59**, R2347 (1999).
[43] R. Gross and A. Frenkel, Nucl. Phys. **A267**, 85 (1976).
[44] C. Fahlander *et al.*, Phys. Rev. C **63**, 021307(R) (2001).
[45] M. Lipoglavšek *et al.*, Phys. Lett. B **440**, 246 (1998).
[46] T. Engeland *et al.*, Phys. Rev. C **61**, 021302(R) (2000).
[47] L. Coraggio *et al.*, J. Phys. G **26**, 1697 (2000).
[48] I. Hamamoto, in *International Symposium on Nuclear Structure Physics*, Göttingen, 2001, edited by R. Casten *et al.* (World Scientific, Singapore, 2001), p. 31.
[49] E. Caurier (private communication).
[50] W. A. Richter *et al.*, Nucl. Phys. **A523**, 325 (1991).